Indonesian Journal of Chemical Science and Technology (IJCST)
State University of Medan, https://jurnal.unimed.ac.id/2012/index.php/aromatika

IJCST-UNIMED 2026, Vol. 09, No. 2, Page; 374 – 386
Received : Jun 19th, 2026 Accepted : Jul 23rd, 2026 Web Published : Jul 31st, 2026

In Silico Evaluation of Nitrogen-Containing Tetrahydropyridine and Piperidine Metabolites Identified from *Strobilanthes tonkinensis* Lindau Leaves as Potential Antibacterial Agents

Hestia Hairima[1]*, Dwi Sapri Ramadhan[2], Dian Wardana[2]

[1] Department of Biology, Faculty of Mathematics and Natural Sciences, Universitas Negeri Medan, Medan 20221, Indonesia
[1] Department of Chemistry, Faculty of Mathematics and Natural Sciences, Universitas Negeri Medan, Medan 20221, Indonesia

*Corresponding author: hestiahrma@unimed.ac.id

ABSTRACT

Strobilanthes tonkinensis Lindau (daun paris), a Southeast Asian aromatic herb, contains several nitrogen-containing piperidine and tetrahydropyridine (THP) metabolites identified by prior GC-MS profiling but not previously evaluated in silico. This study assessed the molecular docking interactions of four such metabolites, 2-propionyl-3,4,5,6-tetrahydropyridine (2-PTHP), 2-acetyl-3,4,5,6-tetrahydropyridine (2-ATHP), 2-(2-furyl)piperidine (2-FP), and 1-(piperidin-2-yl)propan-1-one (PPO) against two bacterial protein targets, FtsA (PDB: 3WT0) and DNA gyrase subunit B (GyrB; PDB: 6KZV), using AutoDock Vina, complemented by ADMET prediction via SwissADME and ProTox 3.0. All four compounds showed moderate binding affinities against FtsA (−5.7 to −5.9 kcal/mol) and GyrB (−5.2 to −6.0 kcal/mol), substantially weaker than the native co-crystallized ligands (−11.5 and −8.9 kcal/mol, respectively). 2-FP exhibited the strongest GyrB affinity (−6.0 kcal/mol) and partially reproduced the native ligand's catalytic-residue contacts (ASP73, ASN46), whereas PPO showed the most catalytically relevant FtsA interaction profile, engaging SER13, VAL211, and ASP210. Structure-activity comparison identified the presence of a piperidine NH (hydrogen bond donor) versus an imine nitrogen as the principal determinant of polar-contact capacity within this scaffold. All compounds fully satisfied Lipinski's Rule of Five, showed high predicted gastrointestinal absorption and blood-brain barrier permeability, and were classified as GHS Acute Oral Toxicity Class IV with inactive predicted hepatotoxicity and carcinogenicity. These findings constitute preliminary computational evidence supporting 2-FP and PPO as candidates for further in vitro antibacterial validation..

Keywords: *Strobilanthes tonkinensis*; molecular docking; tetrahydropyridine; piperidine; ADMET; antibacterial agents

e-ISSN : 2622-4968, p-ISSN : 2622-1349

1. INTRODUCTION

The escalating global burden of antimicrobial resistance (AMR) continues to challenge conventional antibiotic frameworks, with drug-resistant bacterial infections responsible for an estimated 1.27 million deaths worldwide in 2019.[1] The proliferation of multidrug-resistant (MDR) strains of clinically significant pathogens, including *Staphylococcus aureus*, *Escherichia coli*, and *Klebsiella pneumoniae*, has critically reduced the therapeutic efficacy of existing antibiotic classes, underscoring the urgent need for novel scaffolds acting through mechanisms not yet compromised by existing resistance determinants.[2, 3] Medicinal plants remain an important and underexplored reservoir of structurally diverse bioactive natural products with demonstrated or predicted antimicrobial potential.[4]

Among nitrogen-containing heterocyclic scaffolds, tetrahydropyridine (THP) and piperidine derivatives have attracted increasing pharmacological interest for their antimicrobial properties. Acylated THP compounds have been reported to disrupt bacterial metabolic processes and to function as efflux pump inhibitors capable of potentiating conventional antibiotics in *Mycobacterium abscessus*.[5, 6] Synthetic THP analogs have demonstrated antibiofilm activity against *Staphylococcus aureus* in recent structure-activity studies[7], while diverse piperidine-based scaffolds continue to be explored as pharmacophores engaging multiple bacterial protein targets.[8] The nitrogen-containing bicyclic ring system of the THP/piperidine class confers structural rigidity and hydrogen-bond donor/acceptor capability relevant to interaction with polar residues in bacterial enzyme active sites. Despite this broad pharmacological precedent, the structure-activity relationships governing how acyl chain length, ring regiochemistry, degree of unsaturation, and heterocyclic substituent modulate target-binding within this scaffold family have not been systematically examined for plant-derived congeners occurring in naturalistic extract profiles.

Strobilanthes tonkinensis Lindau (Acanthaceae), known locally as *daun paris*, is an aromatic perennial herb of Southeast Asian origin widely used as a culinary flavoring and herbal tea.[9, 10] Its characteristic glutinous-rice aroma is principally attributed to 1-octen-3-ol, benzaldehyde, isophorone, 2-methoxy-3-(2-methylpropyl)-pyrazine, linalool oxide, 1-dodecanol, α-ionone, dan trans-β-ionone, which together account for the majority of the volatile fraction of fresh leaf extracts.[9] A recent comparative GC-MS study of four extraction protocols applied to *S. tonkinensis* leaves, ethanol maceration of fresh and dried leaves, and ethanol and n-hexane Soxhlet extraction of dried leaves, identified a panel of nitrogen-containing piperidine and THP metabolites across the chromatographic profiles, including 2-propionyl-3,4,5,6-tetrahydropyridine (2-PTHP), 2-acetyl-3,4,5,6-tetrahydropyridine (2-ATHP), 2-(2-furyl)piperidine (2-FP), and 1-(piperidin-2-yl)propan-1-one (PPO), in addition to the dominant 2-propionyl-1,4,5,6-tetrahydropyridine (2-THP).[11] While that study subjected 2-THP to molecular docking against three bacterial protein targets, the remaining nitrogen-containing metabolites were not evaluated in silico, leaving their binding potential and pharmacokinetic profiles uncharacterized.

To address this gap, the present study focused on two bacterial protein targets representing distinct and complementary antibacterial mechanisms. FtsA is an actin-like ATPase that functions as a core component of the bacterial divisome, anchoring the tubulin homologue FtsZ to the cytoplasmic membrane and coordinating Z-ring constriction during cytokinesis.[12] Inhibition of FtsA disrupts bacterial cell division through a mechanism orthogonal to classical beta-lactam or fluoroquinolone targets, making it of interest for overcoming resistance to conventional agents. DNA gyrase subunit B (GyrB) harbors the ATPase domain responsible for ATP hydrolysis during DNA supercoiling and is a validated target for antibacterial agents including novobiocin and its synthetic analogs.[13] Blockade of the GyrB ATP-binding pocket prevents DNA replication and transcription. Given the low molecular weight and compact geometry of the THP/piperidine candidates, these targets were

e-ISSN : 2622-4968, p-ISSN : 2622-1349

selected as appropriate receptors for evaluating small-molecule nitrogen heterocycle binding, in contrast to the more extended terpenoid scaffolds examined in the prior study.

The present study therefore aimed to: (1) evaluate the molecular docking interactions of four nitrogen-containing *S. tonkinensis* metabolites, 2-PTHP, 2-ATHP, 2-FP, and PPO against FtsA (PDB: 3WT0) and GyrB (PDB: 6KZV); (2) derive preliminary structure-activity inferences within the THP/piperidine scaffold family by comparison with the previously characterized 2-THP; and (3) assess the pharmacokinetic and toxicological profiles of the candidates via ADMET prediction.

2. MATERIALS AND METHODS

2.1. Compound Selection and Ligand Preparation

Four nitrogen-containing metabolites previously detected by GC-MS analysis of *Strobilanthes tonkinensis* leaf extracts were selected for in silico evaluation.[11] The selection criteria applied in the present study were: (1) structural classification as a piperidine- or tetrahydropyridine-derived metabolite; (2) confirmed identity by GC-MS spectral matching with a NIST library similarity index (SI) ≥ 670; and (3) absence from the set of compounds subjected to molecular docking in the prior study,[11] ensuring non-redundancy of in silico coverage. Given that the focus of the present study is structure-activity exploration within a defined heterocyclic scaffold family, the requirement for detection across a minimum of two independent extraction treatments applied in the prior comparative study to confirm plant-derived origin was not adopted as a criterion here. Instead, structural relationship to 2-THP, which was confirmed across all four extraction treatments, provides pharmacological justification for evaluating each congener regardless of its individual occurrence frequency.

The four compounds selected are summarized in Table 1. Three-dimensional ligand structures in SDF format were retrieved from the PubChem Compound database (https://pubchem.ncbi.nlm.nih.gov) using the respective Compound Identifiers (CIDs). Geometries were subsequently optimized using the MMFF94 molecular mechanics force field implemented in OpenBabel 3.1 prior to docking input preparation.

Table 1. Nitrogen-containing metabolites of *Strobilanthes tonkinensis* selected for in silico evaluation.

No.	Compound	Abbreviation	PubChem CID	Molecular Formula	MW (g/mol)	Detected in Extract(s)[11]
1	2-Propionyl-3,4,5,6-tetrahydropyridine	2-PTHP	522743	$C_8H_{13}NO$	139.19	Fresh EtOH macerate (27.44%); Dried EtOH macerate (2.93%)
2	2-Acetyl-3,4,5,6-tetrahydropyridine	2-ATHP	520300	$C_7H_{11}NO$	125.17	Fresh EtOH macerate (2.15%)
3	2-(2-Furyl)piperidine	2-FP	4715025	$C_9H_{13}NO$	151.21	Fresh EtOH macerate (0.69%)
4	1-(Piperidin-2-yl)propan-1-one	PPO	426124	$C_8H_{15}NO$	141.21	n-Hexane Soxhlet (4.35%)

MW = molecular weight; EtOH = ethanol.

2.2. Protein Target Selection and Preparation

Two bacterial protein targets representing distinct antibacterial mechanisms were selected:

(1) FtsA (*Staphylococcus aureus*; PDB: 3WT0) a bacterial actin-like ATPase essential for cell division.[14] FtsA organizes the divisome complex by anchoring FtsZ to the cytoplasmic membrane; inhibition of its ATP-binding domain disrupts Z-ring formation and cytokinesis.[12]

e-ISSN : 2622-4968, p-ISSN : 2622-1349

(2) DNA gyrase subunit B (GyrB) (*Escherichia coli*; PDB: 6KZV) the ATPase subunit of the type II topoisomerase essential for DNA replication.[15] The GyrB ATP-binding pocket harbors conserved catalytic residues ASP73 and GLU50 and is the site of action of aminocoumarin antibiotics including novobiocin.[13]

Crystal structures were retrieved from the RCSB Protein Data Bank (https://www.rcsb.org). Protein preparation was performed in PyMOL (Schrödinger LLC): co-crystallized water molecules and all heteroatom-containing ligands were removed; polar hydrogen atoms were added and Gasteiger partial charges were assigned to all protein atoms prior to docking file generation.

2.3. Molecular Docking

Molecular docking was carried out using AutoDock Vina 1.2.[16] For each receptor, the docking search space was defined as a three-dimensional grid box centered on the coordinates of the co-crystallized reference ligand, encompassing the known active site:

- 3WT0 (FtsA): center at x = 4.449, y = −6.595, z = 59.105 Å; box dimensions 20 × 20 × 20 Å (ATP-binding cleft region)
- 6KZV (GyrB): center at x = −7.262, y = 15.442, z = 1.646 Å; box dimensions 16 × 15 × 14 Å (GyrB ATP-binding pocket)

Prior to docking of the test compounds, the co-crystallized native ligand of each receptor was re-docked into the prepared protein to validate grid accuracy; an RMSD of ≤ 2.0 Å between the re-docked pose and the crystallographic ligand position was accepted as the validation criterion. The top-ranked binding pose for each compound-receptor pair, as determined by the lowest predicted binding free energy (ΔG, kcal/mol), was recorded and used for all subsequent analyses. A more negative ΔG value indicates stronger predicted non-covalent binding between ligand and receptor.[17]

Binding affinities were interpreted using the classification thresholds applied in the natural product docking literature: moderate (−5.0 to −7.0 kcal/mol), good to strong (−7.0 to −9.0 kcal/mol), and very strong (below −9.0 kcal/mol).[18, 19] For structure-activity comparison within the THP/piperidine scaffold, results were interpreted with reference to the binding affinities previously reported for 2-propionyl-1,4,5,6-tetrahydropyridine (2-THP) at 3WT0 (−5.7 kcal/mol) and 6KZV (−5.4 kcal/mol).

Protein-ligand interaction analyses encompassing conventional and carbon hydrogen bonds, alkyl and π-alkyl contacts, amide-π interactions, salt bridges, attractive charges, and van der Waals forces were performed and visualized using BIOVIA Discovery Studio Visualizer 2024 (Dassault Systèmes).

2.4. ADMET and Drug-Likeness Prediction

Pharmacokinetic properties and drug-likeness of the four candidate compounds were predicted using SwissADME (http://www.swissadme.ch).[20] Canonical SMILES strings for each compound were retrieved from PubChem and used as input. Drug-likeness was evaluated according to Lipinski's Rule of Five, with the following parameters: molecular weight (MW, threshold ≤ 500 g/mol), lipophilicity (XLogP3, threshold ≤ 5), hydrogen bond donors (HBD, threshold ≤ 5), hydrogen bond acceptors (HBA, threshold ≤ 10), and topological polar surface area (TPSA). Predicted gastrointestinal (GI) absorption and blood-brain barrier (BBB) permeability were obtained as pharmacokinetic endpoints. Compounds exhibiting more than one Lipinski violation were considered to have reduced predicted oral bioavailability.[21]

Acute oral toxicity (LD50, mg/kg), hepatotoxicity, and carcinogenicity were predicted using ProTox 3.0 (https://tox.charite.de/protox3/).[22] LD50 values were interpreted using the GHS acute oral toxicity classification: Class I (≤ 5 mg/kg), Class II (5–50 mg/kg), Class III (50–300 mg/kg), Class IV (300–2000 mg/kg), and Class V (2000–5000 mg/kg).

3. RESULTS AND DISCUSSION

3.1. Molecular Docking Validation

e-ISSN : 2622-4968, p-ISSN : 2622-1349

Re-docking of the co-crystallized native ligands into the prepared binding sites of 3WT0 and 6KZV, both below the accepted threshold of 2.0 Å[16], confirming that the defined grid boxes accurately reproduce the crystallographic binding geometry and that the docking protocol is valid for evaluating the test compounds.

3.2. Binding Affinity Overview

The binding free energies (ΔG, kcal/mol) of the four test compounds and their respective native co-crystallized ligand references against both receptors are presented in Table 2. Against FtsA (3WT0), affinities ranged narrowly from −5.7 kcal/mol (2-ATHP) to −5.9 kcal/mol (PPO), all classified as moderate. Against GyrB (6KZV), 2-FP exhibited the strongest binding (−6.0 kcal/mol), while 2-ATHP was weakest (−5.2 kcal/mol). In all cases, test compound affinities remained substantially below those of the native ligands (3WT0: −11.5 kcal/mol; 6KZV: −8.9 kcal/mol), indicating moderate rather than potent predicted inhibitory potential. These findings should therefore be interpreted as preliminary computational evidence of protein-binding capacity, not as predictions of strong inhibitory activity.

Table 2. Binding free energies (ΔG, kcal/mol) of 2-PTHP, 2-ATHP, 2-FP, PPO, and native co-crystallized ligands against FtsA (PDB: 3WT0) and DNA gyrase subunit B (PDB: 6KZV)

Compound	3WT0 (ΔG, kcal/mol)	6KZV (ΔG, kcal/mol)
Native ligand	−11.5	−8.9
2-PTHP	−5.8	−5.3
2-ATHP	−5.7	−5.2
2-FP	−5.8	−6.0
PPO	−5.9	−5.3

2-PTHP = 2-Propionyl-3,4,5,6-tetrahydropyridine; 2-ATHP = 2-Acetyl-3,4,5,6-tetrahydropyridine; 2-FP = 2-(2-Furyl)piperidine; PPO = 1-(Piperidin-2-yl)propan-1-one.

3.2.1 Binding at FtsA (PDB: 3WT0)

FtsA is a bacterial actin-like ATPase essential for divisome assembly, anchoring the tubulin homologue FtsZ to the cytoplasmic membrane and coordinating Z-ring constriction during cytokinesis.[12] Its ATP-binding cleft is formed by polar residues including SER13, SER14, SER15, GLU209, VAL211, ASP210, GLU251, LYS254, GLY325, and ASN328, together with the catalytic magnesium cofactor MG401.[14] The native co-crystallized ligand establishes ten conventional hydrogen bonds with this residue set, supplemented by electrostatic contacts at LYS17 and MG401, accounting for its high affinity of −11.5 kcal/mol. The amino acid interactions of all test compounds and the native ligand at 3WT0 are summarized in Table 3.

Because the binding affinity range across the four test compounds at 3WT0 is only 0.2 kcal/mol (−5.7 to −5.9 kcal/mol), well within the inherent scoring uncertainty of AutoDock Vina of approximately 1–2 kcal/mol, no compound to compound affinity ranking at this target carries statistical significance. Mechanistic interpretation is therefore grounded in the qualitative differences in interaction profiles rather than the numerical ranking of ΔG values.

Table 3. Detailed protein–ligand interaction profile of 2-PTHP, 2-ATHP, 2-FP, PPO, and the native co-crystallized ligand within the active site of FtsA

Receptor	Amino acid	Native Ligand	2-PTHP	2-ATHP	2-FP	PPO
3WT0	SER13					
	SER14					
	SER15					

e-ISSN : 2622-4968, p-ISSN : 2622-1349

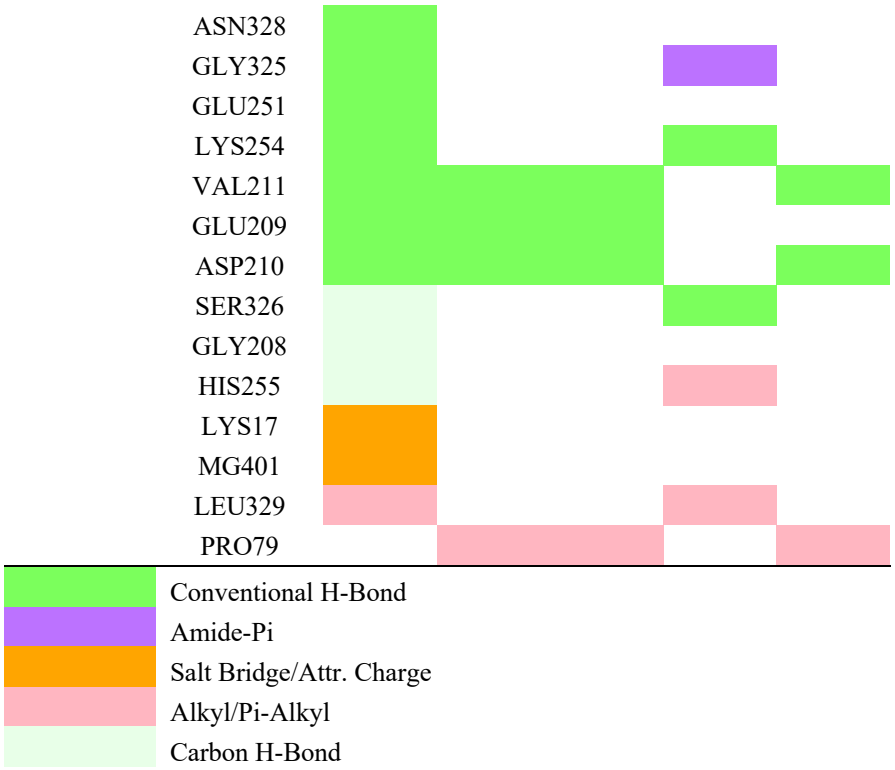

2-PTHP and 2-ATHP each formed only a single explicit interaction at FtsA, namely an alkyl/π-alkyl contact with PRO79 (Figure 1B, 1C). PRO79 is a peripheral hydrophobic residue of the ATP-binding cleft and is not directly implicated in catalysis. The absence of hydrogen bond formation by both compounds is structurally consistent with the imine character of their ring nitrogen (C=N–), which lacks an available proton and consequently has zero hydrogen bond donors (HBD = 0). Binding contributions beyond PRO79 likely derive from non-specific van der Waals contacts with the hydrophobic cleft lining that are not captured as named interactions in Discovery Studio Visualizer but nonetheless contribute to the overall ΔG.

2-FP produced the most chemically diverse interaction profile at 3WT0 despite an affinity identical to 2-PTHP (−5.8 kcal/mol). It established conventional hydrogen bonds with LYS254 and SER326, an amide-π interaction with GLY325, and alkyl/π-alkyl contacts with HIS255, LEU329, and PRO79 (Figure 1D). LYS254 and GLY325 lie within the ATP-binding domain and are residues engaged by the native ligand's extended polar network, indicating partial overlap in binding geometry. The piperidine NH of 2-FP (HBD = 1) is the probable hydrogen bond donor for the LYS254 and SER326 contacts, while the furanyl aromatic ring enables the amide-π interaction with GLY325. That this broader contact repertoire does not translate to higher binding affinity is attributable to the small molecular size of 2-FP (MW = 151.21 g/mol), which limits the total interaction energy achievable regardless of contact diversity.

e-ISSN : 2622-4968, p-ISSN : 2622-1349

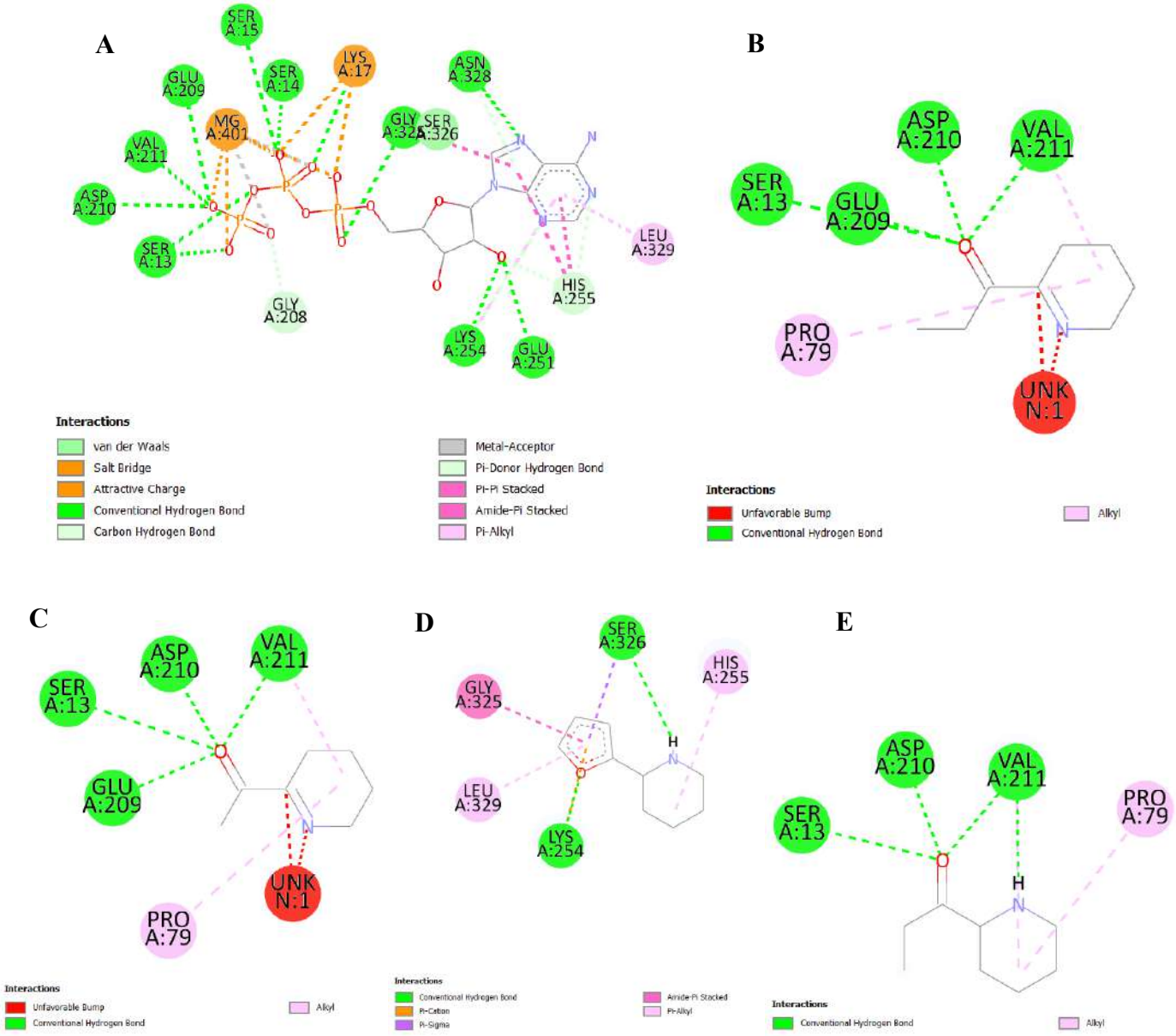

Figure 1. Two-dimensional ligand interaction maps of (A) Native Ligand, (B) 2-PTHP, (C) 2-ATHP, (D) 2-FP, and (E) PPO docked into the active site of FtsA (PDB: 3WT0)

PPO exhibited the most mechanistically relevant interaction pattern at 3WT0 (−5.9 kcal/mol), forming conventional hydrogen bonds with SER13, VAL211, and ASP210, together with an alkyl contact at PRO79 (Figure 1E). SER13 and ASP210 are part of the conserved ATP-coordination residues directly engaged by the native ligand; their involvement in PPO binding indicates partial occupancy of the catalytically relevant binding geometry. The piperidine NH (HBD = 1) and the carbonyl oxygen of the propionyl chain underpin these polar contacts.

For reference, the structurally related 2-THP (2-propionyl-1,4,5,6-tetrahydropyridine, the dominant constituent of fresh *S. tonkinensis* extracts) previously showed a binding affinity of −5.7 kcal/mol at 3WT0 with hydrogen bonds at SER13, GLU209, ASP210, and VAL211, and an alkyl contact at PRO79. PPO (−5.9 kcal/mol) marginally exceeds 2-THP at this target and reproduces H-bond engagement at three of the same catalytic residues (SER13, VAL211, ASP210), differing in that it lacks the GLU209 contact while retaining

e-ISSN : 2622-4968, p-ISSN : 2622-1349

comparable polar coverage. 2-PTHP the direct regioisomer of 2-THP differing only in the position of the ring double bond shows comparable affinity (−5.8 kcal/mol) but a markedly diminished polar interaction profile (PRO79 only), demonstrating that ring regiochemistry governs hydrogen bond donor capacity in this scaffold class: displacement of the double bond from the 1,6- to the 3,4-position shifts the imine nitrogen from a position where the adjacent ring geometry might permit polar contacts, to one where steric or electronic factors restrict interaction to non-polar residues only.

3.2.2 Binding at GyrB (PDB: 6KZV)

The ATP-binding pocket of GyrB contains conserved catalytic residues ASP73 and GLU50, essential for ATP hydrolysis and Mg^{2+} coordination, together with a hydrophobic core comprising ILE78, VAL120, PRO79, ILE94, ALA47, and VAL167.[13, 15] The native co-crystallized ligand engages this pocket through a hydrogen bond with ASP73, an amide-π interaction with ASN46, electrostatic contacts at ARG76 and GLU50, a π-sigma interaction with ILE78, and hydrophobic contacts with VAL120, ILE94, ALA47, and PRO79, achieving a binding affinity of −8.9 kcal/mol. This combination of polar contacts at catalytic residues and hydrophobic pocket filling defines the pharmacophoric requirements for effective GyrB inhibition. The interaction profiles of all test compounds at 6KZV are summarized in Table 4.

Table 4. Detailed protein–ligand interaction profile of 2-PTHP, 2-ATHP, 2-FP, PPO, and the native co-crystallized ligand within the ATP-binding pocket of DNA gyrase subunit B (PDB: 6KZV)

Receptor	Amino acid	Native Ligand	2-PTHP	2-ATHP	2-FP	PPO
6KZV	ASP73	■			■	
	GLY77			■		
	ASN46	■			■	
	ARG76	■				
	GLU50	■				
	ILE78	■	■	■	■	■
	VAL120	■	■		■	■
	ILE94	■				
	ALA47	■			■	
	PRO79	■				
	VAL167		■		■	■
	VAL43				■	■

■ Conventional H-Bond ■ Van Der Waals
■ Amide-Pi ■ Carbon H-Bond
■ Salt Bridge/Attr. Charge
■ Alkyl/Pi-Alkyl
■ Pi-Sigma

2-FP exhibited the strongest binding among the test compounds at 6KZV (−6.0 kcal/mol) and was the only compound to partially reproduce the catalytic site contacts of the native ligand (Figure 2D). It formed a conventional hydrogen bond with ASP73, the catalytic carboxylate essential for ATP hydrolysis, an amide-π interaction with ASN46, a van der Waals contact with ALA47, a conventional hydrogen bond with VAL43, and alkyl/π-alkyl contacts with ILE78, VAL120, and VAL167. The piperidine NH (HBD = 1) is the probable hydrogen bond donor toward ASP73 and VAL43, while the furanyl aromatic ring provides the amide-π contact with ASN46, a contact type also established by the native ligand with the same residue (Figure 2A). The convergence of 2-FP and the native ligand on both ASP73 hydrogen bonding and ASN46 amide-π interaction constitutes partial pharmacophoric mimicry of the native binding mode and is the strongest mechanistic

e-ISSN : 2622-4968, p-ISSN : 2622-1349

rationale for antibacterial potential identified in this study. Compared to the reference compound 2-THP (−5.4 kcal/mol at 6KZV[11]), 2-FP shows a 0.6 kcal/mol improvement accompanied by catalytic residue engagement a difference that survives the AutoDock Vina scoring uncertainty range supporting the furanyl-piperidine scaffold as a superior GyrB-binding motif within this compound family.

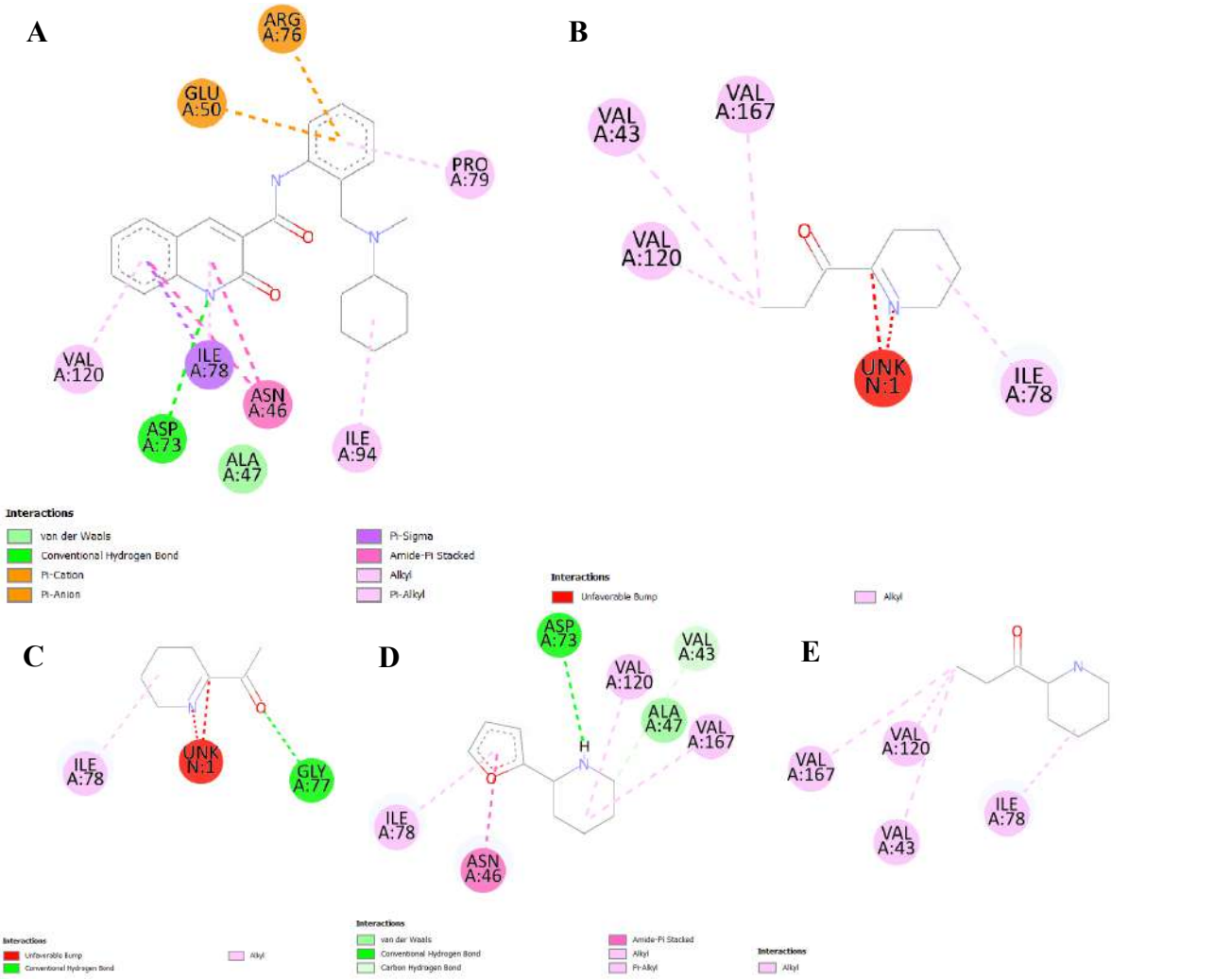

Figure 2. Two-dimensional ligand interaction maps of (A) Native Ligand, (B) 2-PTHP, (C) 2-ATHP, (D) 2-FP, and (E) PPO docked into the ATP-binding pocket of DNA gyrase subunit B (PDB: 6KZV)

PPO (−5.3 kcal/mol) engaged ILE78, VAL120, VAL167, and VAL43 exclusively through alkyl/π-alkyl contacts (Figure 2E). While this occupies the same hydrophobic cleft as the native ligand's non-polar interactions, the complete absence of polar contact with catalytic residues ASP73 or GLU50 limits its predicted mechanistic relevance at this target. This outcome is structurally attributable to the fully saturated piperidine ring and the propionyl carbonyl of PPO, which lacks an aromatic platform for π-type interactions and positions the piperidine NH toward non-catalytic regions of the pocket.

2-PTHP (−5.3 kcal/mol) similarly established only hydrophobic contacts with VAL167 and VAL43 (Figure 2B), consistent with the imine nitrogen character (HBD = 0) restricting interaction to non-polar residues. 2-ATHP (−5.2 kcal/mol) formed a single hydrogen bond with GLY77 (Figure 2C), a non-catalytic glycine backbone residue peripheral to the ATP-binding site. The GLY77 contact, while polar, does not engage

e-ISSN : 2622-4968, p-ISSN : 2622-1349

the catalytic ASP73 or GLU50 machinery and is consistent with a binding pose displaced from the pharmacophoric core. The acetyl chain of 2-ATHP, one methylene unit shorter than the propionyl chain of 2-PTHP, may confer insufficient hydrophobic reach to position the molecule optimally within the pocket, contributing to its lowest binding affinity across both targets.

3.3. Structure-Activity Relationships within the Scaffold

The docking results across both targets permit three preliminary structure-activity inferences within this piperidine/tetrahydropyridine scaffold family. Hydrogen bond donor capacity. The single most consequential structural feature governing interaction profile breadth is the presence or absence of a piperidine NH (HBD = 1) versus an imine nitrogen (HBD = 0). Compounds with a saturated piperidine ring nitrogen (2-FP and PPO, HBD = 1) establish polar contacts with protein residues at both targets, including catalytic site residues SER13, VAL211, and ASP210 at FtsA (PPO) and ASP73 at GyrB (2-FP). In contrast, 2-PTHP and 2-ATHP (HBD = 0, imine C=N–) are restricted to hydrophobic contacts at both targets. This structural difference represents the dominant SAR determinant within this compound set.

Acyl chain length. The propionyl-to-acetyl substitution within the THP subclass (2-PTHP vs. 2-ATHP) produces negligible differences in binding affinity at 3WT0 (−5.8 vs. −5.7 kcal/mol) and only a marginal difference at 6KZV (−5.3 vs. −5.2 kcal/mol), both within scoring uncertainty. Acyl chain extension by a single methylene unit thus provides no binding advantage at either target within this scaffold, suggesting the acyl chain does not contribute directionally to the binding pharmacophore.

Furanyl aromatic substituent. The furanyl ring of 2-FP is the sole structural feature enabling amide-π interactions at both targets (GLY325 at 3WT0; ASN46 at 6KZV) and is critical to the ASP73 hydrogen bond at GyrB, distinguishing 2-FP from all other candidates. These advantages are specific to the aromatic furanyl system and are not replicated by the aliphatic propionyl chain of PPO despite their similar molecular frameworks.

3.4. Drug-Likeness and Pharmacokinetic Properties

The predicted drug-likeness and pharmacokinetic properties of the four test compounds are presented in Table 5. All four compounds fully satisfied Lipinski's Rule of Five with zero violations, consistent with their uniformly low molecular weights (125.17–151.21 g/mol), moderate lipophilicity (XLogP3: −0.08 to 1.27), and low TPSA (25.17–29.43 Å²). All compounds were predicted to exhibit high gastrointestinal absorption and blood-brain barrier (BBB) permeability, reflecting their small MW and low TPSA.

Table 5. Predicted drug-likeness and pharmacokinetic properties of 2-PTHP, 2-ATHP, 2-FP, and PPO obtained from SwissADME analysis.

Compound	MW (g/mol)	XLogP3	TPSA (Å²)	HBA	HBD	GI Absorption	BBB Permeability	Lipinski Violations
2-PTHP	139.19	0.40	29.43	2	0	High	Yes	0
2-ATHP	125.17	-0.08	29.43	2	0	High	Yes	0
2-FP	151.21	1.27	25.17	2	1	High	Yes	0
PPO	141.21	0.90	29.10	2	1	High	Yes	0

MW, molecular weight; XLogP3, predicted octanol/water partition coefficient; TPSA, topological polar surface area; HBA, hydrogen bond acceptors; HBD, hydrogen bond donors; GI absorption, predicted gastrointestinal absorption; BBB permeability, predicted blood–brain barrier permeability.

This uniform Lipinski compliance across all four compounds favorably distinguishes the nitrogen-containing THP/piperidine scaffold from the lipophilic terpenoids evaluated in the companion *S. tonkinensis* study, stigmasterol, phytol, lupeol, and squalene each of which carried one Lipinski violation due to excessive

e-ISSN : 2622-4968, p-ISSN : 2622-1349

lipophilicity (XLogP3 > 5) and showed low predicted GI absorption.[11] The nitrogen-containing alkaloid fraction of *S. tonkinensis* thus offers superior predicted oral pharmacokinetics relative to the lipophilic fraction.

Within the test series, 2-ATHP exhibited the lowest MW (125.17 g/mol) and the sole negative XLogP3 (−0.08), indicating the highest hydrophilicity; however, this correlates with its weakest docking performance at both targets, suggesting the acetyl chain is suboptimally sized for stable binding pocket engagement. 2-FP had the highest XLogP3 (1.27) and lowest TPSA (25.17 Å²), properties attributable to the furanyl aromatic ring, which broadens the hydrophobic contact surface while contributing to π-interaction capacity. The HBD = 1 status of 2-FP and PPO, versus HBD = 0 for 2-PTHP and 2-ATHP, directly correlates with observed hydrogen bond formation in docking and reflects the structural impact of ring nitrogen saturation state on molecular polarity.

3.4. Toxicity Prediction

Acute oral toxicity, hepatotoxicity, and carcinogenicity predictions from ProTox 3.0 are summarized in Table 6. All four compounds were assigned to GHS Acute Oral Toxicity Class IV (LD50 range 300–2000 mg/kg), indicating low acute oral toxicity. PPO showed the highest predicted LD50 (1545 mg/kg), while 2-FP showed the lowest within the group (1000 mg/kg); however, all values remain comfortably within Class IV. Hepatotoxicity and carcinogenicity were predicted as inactive for all compounds, with confidence probability scores ranging from 0.60 to 0.81 across both endpoints.

Table 6. Predicted acute oral toxicity (LD50, mg/kg), GHS toxicity class, hepatotoxicity, and carcinogenicity of 2-PTHP, 2-ATHP, 2-FP, and PPO obtained from ProTox 3.0.

Compound	Predicted LD50 (mg/kg)	Toxicity Class	Hepatotoxicity	Carcinogenicity
2-PTHP	1300	IV	Inactive (0.79)	Inactive (0.60)
2-ATHP	1300	IV	Inactive (0.80)	Inactive (0.61)
2-FP	1000	IV	Inactive (0.73)	Inactive (0.71)
PPO	1545	IV	Inactive (0.67)	Inactive (0.70)

These predictions are in silico estimates and require experimental validation before any toxicological conclusions can be drawn. Nonetheless, the consistent absence of predicted hepatotoxic and carcinogenic activity across all four candidates supports their continued evaluation in experimental antibacterial and safety assays. The phytochemical origin of these compounds in a plant widely consumed as a culinary herb and herbal tea provides contextual plausibility for a generally low-toxicity profile,[9,10] though this qualitative observation does not substitute for empirical data.

Taken together, the molecular docking and ADMET data identify 2-FP as the most promising candidate from the evaluated set, combining the strongest predicted binding at GyrB (−6.0 kcal/mol) with partial pharmacophoric mimicry of the native GyrB inhibitor binding mode, specifically engagement of catalytic residues ASP73 and ASN46, also full Lipinski compliance with high predicted GI absorption. PPO represents the most relevant candidate at FtsA, reproducing hydrogen bonds at three ATP- coordination residues (SER13, VAL211, ASP210) also engaged by the native ligand, albeit at moderate overall affinity. 2-PTHP and 2-ATHP show limited predicted inhibitory interaction profiles at both targets, restricted to peripheral hydrophobic contacts consistent with their HBD = 0 character.

Critically, none of the tested compounds approach the binding strength of the native ligands at either target, and all findings remain at the level of preliminary computational evidence. Further validation through in vitro minimum inhibitory concentration (MIC) determination against *S. aureus* and *E. coli*, GyrB ATPase inhibition assays, and cell membrane permeability studies is required to confirm or refute the antibacterial potential predicted here.

e-ISSN : 2622-4968, p-ISSN : 2622-1349

4. CONCLUSION

Molecular docking of four nitrogen-containing *S. tonkinensis* metabolites against FtsA and GyrB revealed uniformly moderate binding affinities that remained substantially below those of the native co-crystallized ligands at both targets, indicating that none of the tested compounds is predicted to act as a potent inhibitor. Among the candidates, 2-FP was the most promising, combining the strongest predicted GyrB affinity with partial pharmacophoric mimicry of the native ligand through engagement of the catalytic residues ASP73 and ASN46, while PPO showed the most mechanistically relevant FtsA profile via hydrogen bonding with the ATP-coordinating residues SER13, VAL211, and ASP210. Comparative structure-activity analysis indicated that hydrogen bond donor capacity governed by ring-nitrogen saturation state (piperidine NH vs. imine) is the dominant determinant of polar-interaction breadth in this scaffold family, whereas acyl chain length had negligible influence. All four compounds displayed favorable predicted drug-likeness, oral bioavailability, and low acute toxicity. These in silico results should be regarded as preliminary; confirmation of antibacterial potential requires in vitro minimum inhibitory concentration (MIC) testing against *S. aureus* and *E. coli*, GyrB ATPase inhibition assays, and membrane permeability studies, with 2-FP and PPO as priority candidates.

REFERENCES

1. Murray CJL, Ikuta KS, Sharara F, et al (**2022**) Global burden of bacterial antimicrobial resistance in 2019: a systematic analysis. The Lancet 399, 629–655.
2. Puri B, Vaishya R, Vaish A (**2025**) Antimicrobial resistance: Current challenges and future directions. Med J Armed Forces India 81, 247–258.
3. Salam MdA, Al-Amin MdY, Salam MT, Pawar JS, Akhter N, Rabaan AA, Alqumber MAA (**2023**) Antimicrobial Resistance: A Growing Serious Threat for Global Public Health. Healthcare 11, 1946.
4. Newman DJ, Cragg GM (**2020**) Natural Products as Sources of New Drugs over the Nearly Four Decades from 01/1981 to 09/2019. J Nat Prod 83, 770–803.
5. Ramis IB, Vianna JS, Silva Junior L, von Groll A, Ramos DF, Lobo MM, Zanatta N, Viveiros M, Silva PEA da (**2019**) In silico and in vitro evaluation of tetrahydropyridine compounds as efflux inhibitors in Mycobacterium abscessus. Tuberculosis 118, 101853.
6. Vianna JS, Ramis IB, Bierhals D, von Groll A, Ramos DF, Zanatta N, Lourenço MC, Viveiros M, Almeida da Silva PE (**2019**) Tetrahydropyridine derivative as efflux inhibitor in Mycobacterium abscessus. J Glob Antimicrob Resist 17, 296–299.
7. Chaudhary G, Verma A, Maurya S, Singh R, Tyagi S, Manna B, Katara P, Prabhakar A, Verma D, Bihari Yadav A (**2026**) Design, Synthesis, and Biological Evaluation of Tetrahydropyridine Analogues as Potent Antibiofilm Agents against *S. aureus* : In Vitro and In Silico Studies. ACS Omega 11, 476–489.
8. Rossetti A, Bono N, Candiani G, Meneghetti F, Roda G, Sacchetti A (**2019**) Synthesis and Antimicrobial Evaluation of Novel Chiral 2-Amino-4,5,6,7-tetrahydrothieno[2,3- *c*]pyridine Derivatives. Chem Biodivers. https://doi.org/10.1002/cbdv.201900097
9. Hua J, Li J, Ouyang W, Wang J, Yuan H, Jiang Y (**2022**) Effect of Strobilanthes tonkinensis Lindau Addition on Black Tea Flavor Quality and Volatile Metabolite Content. Foods 11, 1678.
10. Yang X, He X, Cui Y, Ji L, Hu J, Hao J, He B (**2025**) Enhance rice-like aroma of on *Strobilanthes tonkinensis* var. *tonkinensis* extract using hydroxypropyl- *β* -cyclodextrin. Int J Food Prop. https://doi.org/10.1080/10942912.2025.2595770
11. Ramadhan DS, Wardana D, Hairima H, Juwitaningsih T, Nadya R, Sitorus E, Azzahra VO, Sinuraya I (**2026**) GC-MS Profiling and In Silico Antibacterial Activity of Strobilanthes tonkinensis Lindau Leaf Extracts via Maceration and Soxhlet Methods 2. Biology, Medicine, & Natural Product Chemistry 15:
12. Cameron TA, Margolin W (**2023**) Construction and Characterization of Functional FtsA Sandwich Fusions for Studies of FtsA Localization and Dynamics during Escherichia coli Cell Division. J Bacteriol. https://doi.org/10.1128/jb.00373-22
13. Gupta D, Tiwari P, Haque MA, Sachdeva E, Hassan MI, Ethayathulla AS, Kaur P (**2021**) Structural insights into the transient closed conformation and pH dependent ATPase activity of S.Typhi GyraseB N- terminal domain. Arch Biochem Biophys 701, 108786.
14. Kato K, Ishido T, Matsui T, Yao M (**2015**) Crystal Structure Analysis of Cell Division Protein. Worldwide Protein Data Bank. https://doi.org/10.2210/pdb3wt0/pdb

e-ISSN : 2622-4968, p-ISSN : 2622-1349

15. Mima M, Ushiyama F (**2020**) Crystal structure of E.coli DNA gyrase B in complex with 2-oxo-1,2-dihydroquinoline derivative. Worldwide Protein Data Bank. https://doi.org/10.2210/pdb6kzv/pdb
16. Trott O, Olson AJ (**2010**) AutoDock Vina: Improving the speed and accuracy of docking with a new scoring function, efficient optimization, and multithreading. J Comput Chem 31, 455–461.
17. Liu W, Liu Z, Liu H, Westerhoff LM, Zheng Z (**2022**) Free Energy Calculations Using the Movable Type Method with Molecular Dynamics Driven Protein–Ligand Sampling. J Chem Inf Model 62, 5645–5665.
18. Boufissiou A, Abdalla M, Kadi I, et al (**2025**) Identification of natural product inhibitors as potential drug candidates for treating Alzheimer's disease: molecular docking, molecular dynamics simulations, MM/GBSA and pharmacokinetics. Network Modeling Analysis in Health Informatics and Bioinformatics 14, 56.
19. Hartavi A (**2025**) Onosma obtusifolia extracts: Antioxidant potential and molecular docking insights into acetylcholinesterase, α-amylase, and tyrosinase inhibition. Ind Crops Prod 233, 121387.
20. Daina A, Michielin O, Zoete V (**2017**) SwissADME: a free web tool to evaluate pharmacokinetics, drug-likeness and medicinal chemistry friendliness of small molecules. Sci Rep 7, 42717.
21. Lipinski CA, Lombardo F, Dominy BW, Feeney PJ (**2001**) Experimental and computational approaches to estimate solubility and permeability in drug discovery and development settings 1PII of original article: S0169-409X(96)00423-1. The article was originally published in Advanced Drug Delivery Reviews 23 (1997) 3–25. 1. Adv Drug Deliv Rev 46, 3–26.
22. Banerjee P, Kemmler E, Dunkel M, Preissner R (**2024**) ProTox 3.0: a webserver for the prediction of toxicity of chemicals. Nucleic Acids Res 52, W513–W520.

e-ISSN : 2622-4968, p-ISSN : 2622-1349